JOURNAL OF Materials CHEMISTRY

Electrochemical reaction of lithium with the $CoSb_3$ skutterudite

Ricardo Alcántara,†[a] Francisco J. Fernández-Madrigal,[a] Pedro Lavela,[a] José L. Tirado,*[a] Jean Claude Jumas[b] and Josette Olivier-Fourcade[b]

[a]*Laboratorio de Química Inorgánica, Facultad de Ciencias, Universidad de Córdoba, Avda. San Alberto Magno s/n, 14004 Córdoba, Spain. E-mail: iq1ticoj@lucano.uco.es*
[b]*Laboratoire de Physicochimie de la Matière Condensée (UMR 5617 CNRS), Place Eugène Bataillon, 34095 Montpellier Cedex 5, France*

Received 16th March 1999, Accepted 9th June 1999

The crystalline solid $CoSb_3$ with the skutterudite structure was used as the starting cathodic material in Li|$LiClO_4$(propylene carbonate–ethylene carbonate)|$CoSb_3$ cells. The galvanostatic discharge takes place in two successive plateaux around 0.5 V, leading to a maximum capacity of *ca.* 800 mA h g^{-1}. Further cycling leads to higher voltages and a reversible capacity in the range 350–200 mA h g^{-1} during the first 10 cycles. The mechanism of the reaction with lithium was studied by X-ray diffraction and FTIR spectroscopy. The first discharge involves the irreversible decomposition of the solid to non-crystalline cobalt and Li_3Sb alloy. On cycling, the reversible extraction–insertion of lithium in the antimony alloy takes place. Part of the irreversible capacity is ascribable to the formation of a passivating film on the surface of the electrode material, which contains $ROCO_2^-$ and CO_3^{2-} groups. This material shows superior properties relative to a pure antimony electrode and can be considered as an interesting candidate for the negative electrode of lithium-ion cells.

Introduction

Cobalt triantimonide is one of the transition metal pnictides which belongs to the skutterudite family. Structurally, skutterudites are part of a larger group of cubic solids which can derived from the general $Pm\bar{3}m$ ABX_3 perovskite structure by tilting each octahedron through a fixed angle ϕ.[1] The resulting distortion leads to two different types of A atoms: A′ and A″, and increases the unit cell volume by four times. Accordingly, the crystal symmetry is now described by the $Im\bar{3}$ space group and the unit cell contents are now $A'A''_3B_4X_{12}$. Vacancies in both A′ and A″ sites lead to solids isostructural with the mineral skutterudite $CoAs_3$.[1–4] This solid is also related to ReO_3 by tilting of the octahedra through ϕ (Fig. 1). In $CoSb_3$, as in skutterudite itself, cobalt atoms are the B atoms, which occupy 8c sites of the $Im\bar{3}$ unit cell. Antimony atoms are the X atoms in the structure and occupy 24g sites, in which y and z coordinates are given by $(3\cos\phi \pm \sqrt{3}\sin\phi)/(8\cos\phi + 4)$. For $CoSb_3$, the values reported by Kjekshus, Nicholson and Rakke[5] for these coordinates were $y = 0.344$ and $z = 0.160$, which gives $\phi \approx 35°$.

From the point of view of their applications, an increasing number of skutterudite antimonides are receiving detailed examination owing to their potentially efficient thermoelectric behaviour. Binary ($CoSb_3$) and multicomponent [$LaFe_{4-x}Co_xSb_{12}$ $(0 < x < 4)$] skutterudite antimonides were found to be particularly promising.[6]

In recent years, there has been great interest in the study of lithium alloys with the aim of finding new materials for the negative electrode of lithium-ion cells, as an alternative to carbon based materials.[7] In particular, tin alloys have received prominence due to the large reversible capacities which can be obtained for the highly dispersed metal.[8] Some of the pioneering work on the performance of lithium alloys was carried out by Weppner and Huggins who first reported the coulometric titration of Sb with Li at 400 °C in a molten salt electrolyte.[9] Later, Wang *et al.*[10] reported the potential *vs.* composition curves for antimony alloys at 25 °C, and observed a plateau at *ca.* 0.95 V for Li_3Sb. Several alloys in the Sn–Sb,[11,12] Cu–Sn,[13] Fe–Sn[14] and Fe–Sn–C[15] systems have also been the subject of study as lithium storage materials for lithium-ion batteries. To our knowledge, the use of $CoSb_3$ as the active electrode material in lithium anode or lithium-ion cells has not been reported. Here, we evaluate the cycling performance and discharge properties of this solid.

Experimental

$CoSb_3$ was prepared as follows: stoichiometric amounts of the elements (Aldrich) were weighed, intimately mixed by extensive grinding and placed in silica tubes sealed under vacuum. The tubes were slowly heated to 750 °C, this temperature was maintained for seven days and then the tubes allowed to cool to

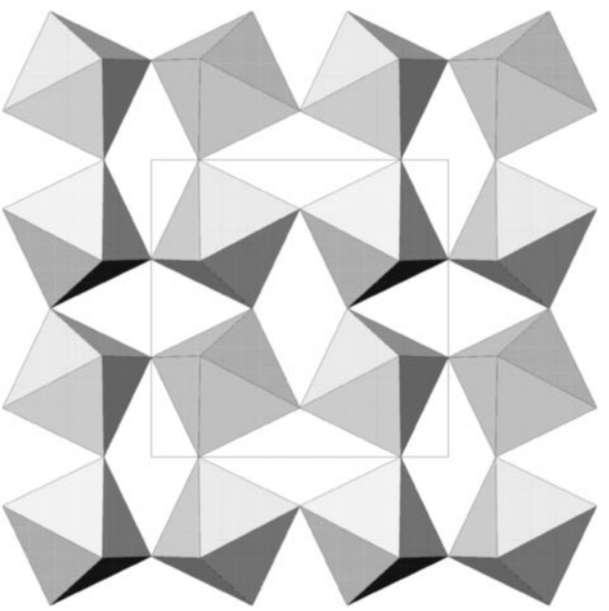

Fig. 1 Projection of the $CoSb_6$ octahedra along [001] in the structure of $CoSb_3$.

†Present address: SAFT Research Laboratories, 111–113 Boulevard Alfred Daney, 33074 Bordeaux Cedex, France.

room temperature over three days, and the product ground. The phase purity of the powder product was evaluated by XRD using a Siemens D5000 diffractometer with monochromated Cu-Kα radiation by using step scans of 0.05° 2θ step size and 20 s duration. The unit cell parameters were refined by using a computer program (AFFMA).[16] FTIR spectra were obtained using a Bomem 300 spectrometer under transmittance conditions.

For the electrochemical studies of lithium cells, 7 mm diameter cathodes of $CoSb_3$ were obtained by pressing $CoSb_3$ (82 wt%), PTFE binder (12 wt%) and carbon black 4N Strem (6 wt%) on a steel iron network substrate. Cells were assembled in a argon glove box using $CoSb_3$ and lithium as electrodes and 1M $LiClO_4$ in PC–EC (1 : 1, v/v) as electrolyte. Electrochemical experiments were carried out using a galvanostat/potentiostat multichannel Mac Pile system. The modified cathode electrodes described above were also tested in a lithium cell.

Results and discussion

Fig. 2 shows profiles of the discharge and charge branches of a lithium anode battery Li|$LiClO_4$(PC + EC)|$CoSb_3$ using currents of 50 or 30 μA. During the first discharge, two successive regions can be observed as plateaus separated by a slight but well defined change in voltage at *ca.* 250 mA h g^{-1} [*ca.* 4.0 F mol^{-1} ($CoSb_3$)]. The first step was shown to be irreversible, as attempts to charge the cell from depths of discharge below 5 F mol^{-1} resulted in a rapid cell polarization. By contrast, a reversible capacity could be observed after allowing the cell to be discharged to 0 V, which was achieved for a depth of discharge of *ca.* 800 mA h g^{-1} ($CoSb_3$). The first few cycles shown in Fig. 2 reveal an initial reversible capacity of *ca.* 400 mA h g^{-1}. Also, a highly reproducible shape for the consecutive charge and discharge branches is obtained after the first discharge. The inset in Fig. 2 indicates that capacity retention is particularly good from cycle 3 to 20, with cell capacities close to 200 mA h g^{-1}. Both the working voltage of the electrode *vs.* lithium and the cycling performance make this material an interesting candidate for the negative electrode of batteries based on lithium-ion technology.

In a closer inspection of Fig. 2, it should be noted that the voltage at which the discharge branches of the second and successive cycles occur is larger than that observed in the second step of the first discharge. Such behaviour may be indicative of a different chemical process during the first reduction process, as compared with further discharges. Thus the characterization of the products obtained by interrupting the galvanostatic experiments at different points of the curve in Fig. 2 was carried out.

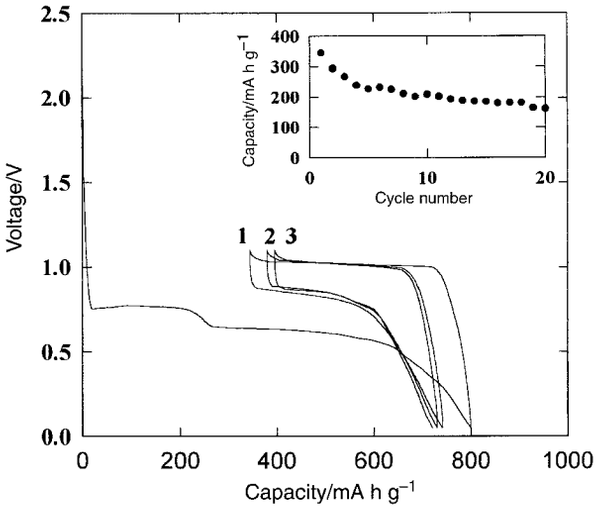

Fig. 2 Cycling profiles of Li/$LiClO_4$(PC + EC)/$CoSb_3$ cells using currents of 30 and 50 μA during charge and discharge, respectively. Inset: cell capacity *vs.* cycle number.

Fig. 3 shows the XRD pattern of the pristine material recorded from the mounted electrode pellet with carbon black additives, PTFE binder and the same plastic cover used in the discharged electrodes to avoid exposure to air. The reflection bands ascribable to the amorphous additives occurred below $2\theta = 35°$. The refinement of the cubic unit cell parameter leads to $a = 9.011_4$ Å ($V = 731.8$ Å^3), which is in good agreement with the value reported by Kjekshus *et al.*[5] This value can be converted to the octahedral tilting angle ϕ by using the Co–Sb distance (d) reported by the same authors, by use of eqn. (1).

$$\cos\phi = [3(a/d) - 4]/8 \quad (1)$$

From this simple expression, a value of $\phi = 32.7_5°$ is obtained, which differs from that of the ideal collapsed perovskite structure ($\phi = 22.24°$, Fig. 1).[1]

Fig. 3 also shows the XRD pattern for the electrode discharged at 110 and 220 mA h g^{-1} [*i.e.* 1.74 and 3.48 F mol^{-1} ($CoSb_3$)]. These data show that the lines ascribable to the skutterudite structure are still visible during after the first discharge step, although a significant decrease in the line intensities and an increase in the signal to background ratio were observed, which can be ascribed to a progressive amorphization. The loss of long range order is clearly observed in XRD patterns of the electrode discharged to 660 mA h g^{-1} [*i.e.* 10.4 F mol^{-1} ($CoSb_3$)].

The unit cell parameter of the skutterudite-related solid obtained after partial reduction was evaluated by the refinement procedure, leading to $a = 8.995_6$ Å. The difference from the initial value falls is in the range of experimental errors associated to this measurement and thus cannot be considered significant, *i.e.* the skutterudite solid which is present at this depth of discharge shows no clear expansion. Moreover, assuming that the d(Co–Sb) distances are unaffected by the

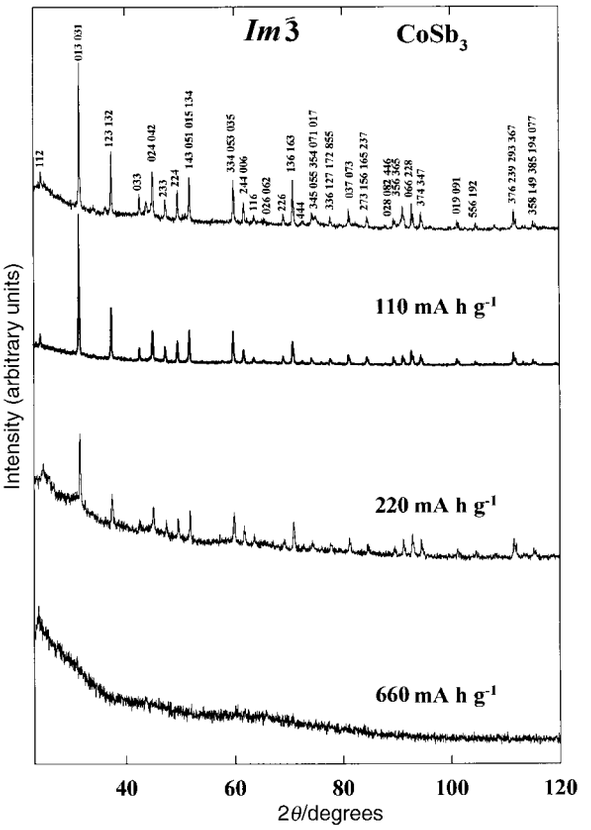

Fig. 3 XRD patterns of the pristine material, and the electrode discharged to 110, 220 and 660 mA h g^{-1}.

partial reduction, a value of $\phi = 33.0_6^\circ$ is obtained which is not significantly different from the initial value. Nevertheless these observations cannot be directly used to discard a possible mechanism based on the intercalation of lithium in the interstices defined by the $CoSb_6$ octahedra, as described by eqn. (2).

$$CoSb_3 + xLi \rightarrow Li_xCoSb_3 \quad (2)$$

In fact, the size of the interstitial sites (A′ and A″ sites in the $A'A''_3B_4X_{12}$ distorted perovskite) are large enough to allow the incorporation of lithium ions without any marked distortion of the lattice. However, a detailed study of the relative intensities of the diffraction lines revealed that these were basically unaffected. Although the scattering factor of lithium is low for X-rays when compared with heavier atoms such as Co and Sb, a simulation of how the intensities could be affected by the insertion of lithium was carried out by using LAZY-PULVERIX[17] software. The calculated values showed slight but significant changes, *e.g.* 7.1% variation for the intensity of the (211) lines, on allowing lithium atoms into the A′ (2a) and A″ (6b) sites as would result from the hypothetical reaction (2). However, from this analysis by comparison with the experimental XRD profiles, which are particularly broadened in the reduced electrode, conclusive proof of intercalation cannot be obtained. Nevertheless, the lack of lattice expansion can be taken as an indirect proof of the absence of insertion, as this result contrasts with the observed behaviour of the binary antimonide InSb, for which a unit cell volume expansion of *ca.* 4.4% led to the proposal of a lithium intercalation mechanism by reaction with *n*-butyllithium.[18]

From the above discussion, it can be inferred that the two-step discharge shown in Fig. 2 involves at least two different processes: collapse of the skutterudite structure and reaction of lithium with the amorphous products. The second process requires the existence of new non-crystalline binary or ternary phases in the Li–Co–Sb system. To our knowledge, no ternary phase has been described in this system. Moreover, according to published phase diagrams, cobalt is not prone to form alloys with lithium, at least for Li contents >0.1 atom% in the temperature range 500–700 °C.[19] However, Hashimoto[20] reported a solid solubility of Li in Co of *ca.* 30 atom% at the ε-Co to α-Co transformation temperature.

By contrast, several phases have been identified in the binary Li–Sb system. Thus, it is well established that Li_2Sb can be prepared by direct reaction of the elements,[21] and Li_3Sb can be obtained from reaction of the elements in liquid ammonia and shows a phase change from the room temperature α-modification to a β-Li_3Sb modification at 650 °C.[22] By use of electrochemical procedures carried out at 350–600 °C, both compounds could be obtained.[9] Room temperature experiments allowed identification of two potential values corresponding to the different domains $Li_{2-3}Sb$ (0.948 V) and $Li_{1-2}Sb$ (0.956 V).[23] The complete discharge process may then be written in terms of eqns. (3) and (4).

$$CoSb_3 + 6\ Li \rightarrow 3\ Li_2Sb + Co \quad (3)$$

$$CoSb_3 + 9\ Li \rightarrow 3\ Li_3Sb + Co \quad (4)$$

These two reactions should take place at below 0.948 V under the dynamic conditions of the experiment shown in Fig. 2, as a result of the exoergic formation of $CoSb_3$ expected from the ΔH°_f value [$\Delta H^\circ_f(CoSb_3) = -16$ kcal mol^{-1}] and the small entropy changes in solids.[24] Following the first discharge, the reversible extraction of lithium from the alloy with antimony may occur in further cycles, which can be related to the following alloy formation–decomposition processes [eqn. (5)].

$$3\ Li_2Sb + 3\ Li \rightleftarrows 3\ Li_3Sb\ (\text{per mol of } CoSb_3) \quad (5)$$

The fact that this process takes place at room temperature without marked polarization can be related to the finely dispersed nature of the antimony clusters on the non-crystalline cobalt matrix.

The above interpretation fails to explain the total capacity of the lithium cells using $CoSb_3$ as the initial cathode material. While a maximum capacity of 9 F mol^{-1} is expected during the first discharge by assuming only eqn. (4), the experimental value is surprisingly larger [*ca.* 13 F mol^{-1} (see Fig. 2)]. The difference is not easily rationalized even admitting a 30 atom% alloying process with cobalt. Two alternative mechanisms may be proposed to explain this divergence: (i) the formation of a passivating layer as a result of the reaction of lithium with the electrolyte at the surface of the metal particles, and (ii) the insertion of lithium within 'cavities' defined by the particles of the electrode material. Both mechanisms have been proposed in carbon-based electrodes working at similar low potentials. Mechanism (ii)[25] should lead to a chemical potential of the inserted lithium close to that of metallic lithium,[26] which is not the case in the plots of Fig. 2. Thus mechanism (i) is more likely to occur in the antimony alloys and cobalt surfaces. The nature of the passivating layer has been the subject of an intense debate. Dey[27] proposed that the protective film on Li electrodes was Li_2CO_3. On the other hand, FTIR spectra of lithium, Li_xC_6 and noble metal surfaces polarized to low potentials in lithium salt solutions in PC indicated the occurrence of $ROCO_2Li$ species resulting from solvent reactions.[28] XPS data revealed a strong dependence on the nature of the solvent and the

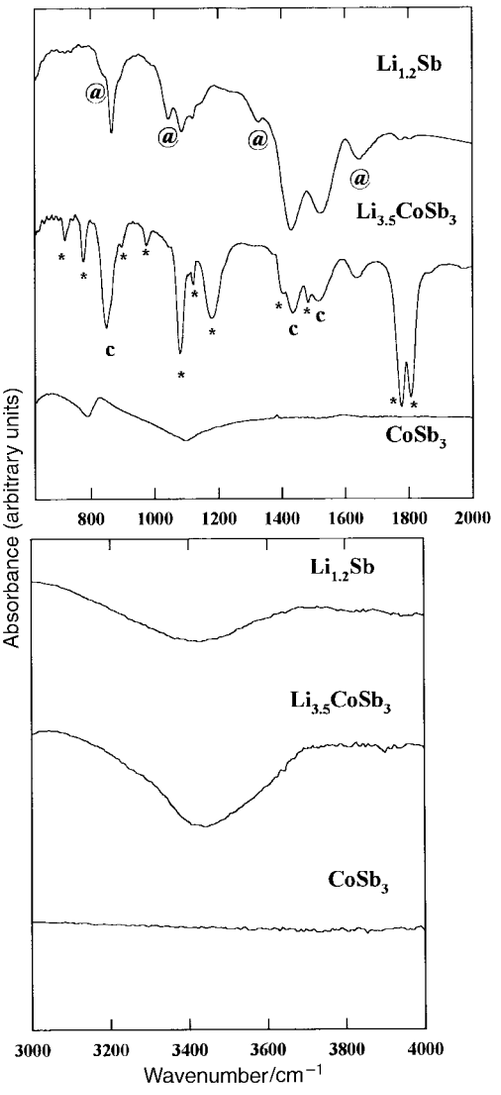

Fig. 4 FTIR spectra of pristine $CoSb_3$, $Li_{3.5}CoSb_3$ and $Li_{1.2}Sb$ electrodes. Bands ascribable to (*) PC and EC; (c) CO_3^{2-} groups; (@) RCO_2Li species.

formation of LiOH films at the surface of carbon electrodes.[29] Nevertheless, ^{6}Li MAS NMR data have shown the ionic nature of lithium on the surface of coke electrodes.[30]

The *ex situ* FTIR spectrum for $Li_{3.5}CoSb_3$ is shown in Fig. 4 and compared with the pristine solid. The spectrum of the discharged electrode material was recorded without rinsing with solvent to avoid any modification of the composition of the surface constituents. A complex diagram with multiple IR peaks can be observed, in which the bands corresponding to the PC–EC mixture used as the electrolyte solvent are clearly visible (marked by asterisks in Fig. 4).[31] The remaining peaks can be ascribed to the simultaneous occurrence of both lithium carbonate and $ROCO_2Li$ species. First, three intense signals at 849, 1435 and 1516 cm^{-1} are in good agreement with early results obtained by Aurbach *et al.*[32] for passivating films of Li_2CO_3 on Li_xC_6 electrodes when using a PC–$LiAsF_6$ electrolyte. Additionally, two low-intensity IR peaks are visible at 1636 and 1320 cm^{-1} which can be ascribed to the $-OCO_2^-$ group of $ROCO_2Li$. This group would be expected to arise from a one-electron reduction of the PC–EC molecules in contact with the surface of the lithiated alloy at a particularly low potential. Moreover, the vibrational modes ν(C–O) at 1070–1100 cm^{-1} and $\delta(CO_3^-)$ at 820–840 cm^{-1}, also characteristics of $-OCO_2^-$ species, occur as shoulders of other more intense signals of the spectrum. In order to interpret the presence of both CO_3^{2-} and $-OCO_2^-$ in the passivating layer, it should be noted that the presence of traces of water during the *ex situ* FTIR recordings could be responsible [eqn. (6)]

$$2\,ROCO_2Li + H_2O \rightarrow Li_2CO_3 + CO_2 + ROH \qquad (6)$$

leading to the more intense signals due to lithium carbonate. Furthermore, the presence of a broad band at 3440 cm^{-1} in the spectra of the discharged electrode, not visible in the pristine solid, could be taken as an indirect evidence of this reaction. Nevertheless, a mechanism based on the formation of LiOH by the reaction of water with $LiClO_4$–PC similar to that described in graphitized MCMBs (meso carbon micro beads)[29] cannot be discarded. In any case, the negligible differences in the XRD patterns of the electrodes from the first to the second plateau, *i.e.* from 110 to 220 mA h g^{-1} (Fig. 3), are in accord with the FTIR results and the interpretation given to the first plateau in terms of the formation of a non-crystalline passivating layer.

Further insight about the reduction mechanism of skutterudite electrodes was obtained by recording cycling curves of lithium cells using polycrystalline antimony as the initial active cathode material. The cells were constructed under the same experimental conditions as for skutterudite. Fig. 5 shows the extended plateau corresponding to the formation of the alloy. Moreover, the X-ray diffraction patterns of the electrode

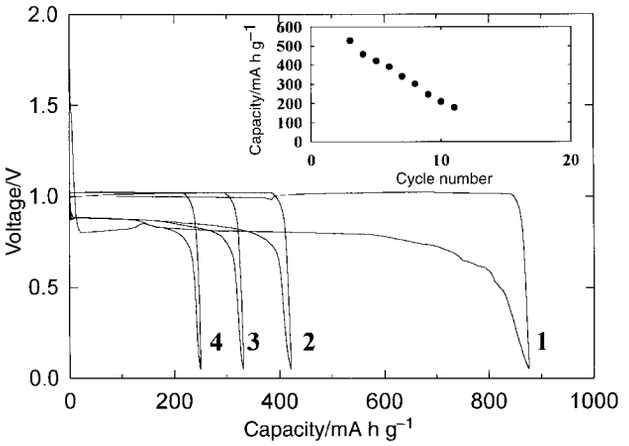

Fig. 5 Cycling profiles of Li/$LiClO_4$(PC+EC)/Sb cells using currents of 30 and 50 μA during charge and discharge, respectively. Inset: cell capacity *vs.* cycle number.

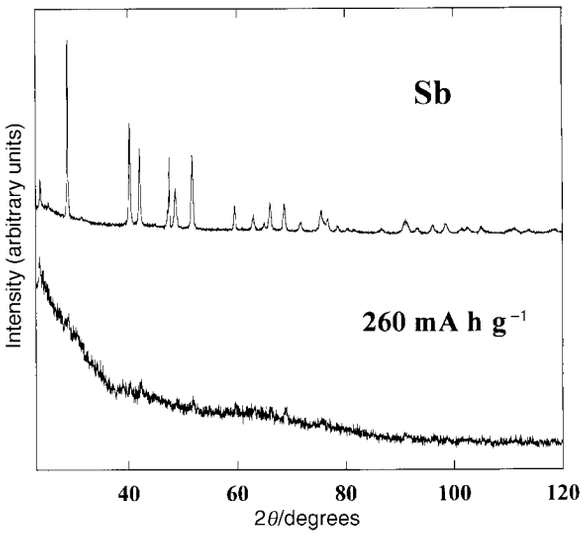

Fig. 6 XRD patterns of pristine antimony and of the electrode discharged to 260 mA h g^{-1}.

discharged to 260 mA h g^{-1} also indicated an almost complete loss of long-range order during the formation of the antimony alloy (Fig. 6). The final capacity is again larger than that expected from eqn. (7).

$$Sb + 3\,Li \rightarrow Li_3Sb \qquad (7)$$

The FTIR spectrum of $Li_{1.2}Sb$ (Fig. 4) gives new insight to the origin of the irreversible capacities. First, the less pronounced IR peaks ascribable to the solvent allow us to confirm the band assignment given above. As a consequence, the peaks for $ROCO_2Li$ species are better resolved. Thus, the peak located at 1050 cm^{-1} and the shoulder at *ca.* 840 cm^{-1} confirm the presence of these lithiated species.

In addition, from Fig. 5 it should be noted that the performance of the antimony electrodes is comparable with that of $CoSb_3$ during the first four cycles (Fig. 2). However the capacity retention is poorer on prolonged cycling (*e.g.* 177 mA h g^{-1} in cycle 10 for Sb *cf.* 208 mA h g^{-1} in cycle 10 and 180 mA h g^{-1} in cycle 18 for $CoSb_3$). This phenomenon could be a consequence of the different state of dispersion of antimony atoms in both materials. The detrimental effect on cell performance upon aggregation through cycling has also been reported in SnO-containing glasses.[33] Thus, the antimony atom clusters formed after the first discharge of $CoSb_3$ suffer less marked changes during prolonged cycling.

Conclusion

$CoSb_3$, one of the members of the skutterudite family of perovskite-related solids, was used as the starting electrode material in lithium batteries. The cells were constructed by using a $LiClO_4$–PC electrolyte. The working cell potential was always below 1.5 V, which makes this material an interesting candidate for the negative electrode of lithium-ion cells. A maximum capacity of *ca.* 800 mA h g^{-1} is obtained during the first cell discharge, which takes place by two successive plateaus at *ca.* 0.5 V. Further charge and discharge processes take place at *ca.* 1.2 and 0.8 V, respectively. The reversible capacity is *ca.* 350 mA h g^{-1} for the first cycle, and decreases to *ca.* 200 mA h g^{-1} after 20 cycles. The amorphization of the electrode material through the first discharge and the phase diagrams of the Li–Sb system published in the literature suggest that the skutterudite structure does not intercalate lithium. Instead the irreversible decomposition of the solid to non-crystalline cobalt and Li_3Sb alloy takes place during the first discharge. Further cycles involve the reversible extraction–

insertion of lithium in the antimony alloy. The capacity retention is better than in pure antimony electrodes, probably due to the dispersion of the metal caused by the decomposition of skutterudite. Finally, part of the irreversible capacity is ascribable to the formation of a passivating film on the surface of the electrode material. As revealed by FTIR, the passivating film mainly consists of the products of one- and two-electron reduction of propylene carbonate and ethylene carbonate.

Acknowledgements

The authors acknowledge financial support from CICYT and Universidad de Córdoba. R. A. thanks the CNRS for a 'Poste Rouge'.

References

1 B. G. Hyde and S. Andersson, *Inorganic Crystal Structures*, J. Wiley & Sons, New York, 1989, p. 299.
2 I. Oftedal, *Z. Kristallogr.*, 1928, **66**, 517.
3 E. H. Roseboom, *Am. Mineral.*, 1962, **47**, 310.
4 N. Mandel and J. Donuohe, *Acta Crystallogr., Sect. B*, 1971, **27**, 2288.
5 A. Kjekshus, D. G. Nicholson and T. Rakke, *Acta Chem. Scand.*, 1973, **27**, 1307.
6 B. C. Sales, D. Mandrus and R. K. Williams, *Science*, 1996, **272**, 1325.
7 K. Sawai, Y. Iwakoshi and T. Ohzuku, *Solid State Ionics*, 1994, **69**, 273.
8 I. A. Courtney and J. R. Dahn, *J. Electrochem. Soc.*, 1997, **144**, 2045.
9 W. Weppner and R. A. Huggins, *J. Electrochem. Soc.*, 1978, **125**, 7.
10 J. Wang, I. D. Raistrick and R. A. Huggins, *J. Electrochem. Soc.*, 1986, **133**, 457.
11 J. O. Besenhard, J. Yang and M. Winter, *J. Power Sources*, 1997, **68**, 87.
12 J. Yang, M. Wachtler, M. Winter and J. O. Besenhard, *Electrochem. Soc. Lett.*, 1999, **2**, 161.
13 J. T. Vaughey, K. D. Kepler and M. M. Thackeray, *Ext. Abstr., No. 82, 9th Int. Symp. Lithium Batteries*, Edinburgh, Scotland, July 1998.
14 O. Mao, R. A. Dunlap, I. A. Courtney and J. R. Dahn, *J. Electrochem. Soc.*, 1998, **145**, 4195.
15 O. Mao, R. A. Dunlap and J. R. Dahn, *J. Electrochem. Soc.*, 1999, **146**, 405.
16 J. Rodríguez Carvajal, AFFMA, Program for the refinement of unit cell parameters, ILL, Grenoble, France, 1987.
17 K. Yvon, W. Jeitschko and E. Parthé, LAZY-PULVERIX, Program for the simulation of XRD patterns, University of Geneva, Switzerland, 1987.
18 G. Herren and N. E. Walsöe de Reca, *Solid State Ionics*, 1991, **47**, 57.
19 M. Bonnemay, E. Levart, G. Bronoel, B. Peslerbe and M. Savy, *Mém. Sci. Rev. Métall.*, 1965, **62**, 285.
20 U. Hashimoto, *Nippon Kinzoku Gakkai-Shi*, 1937, **1**, 177.
21 R. Gerardin and J. Aubry, *C. R. Acad. Sci., Ser. C.*, 1974, **278**, 1097.
22 G. Brauer and E. Zintl, *Z. Phys. Chem., Abt. B*, 1937, **37**, 323.
23 R. A. Huggins in, *Batteries for portable applications and electric vehicles*, ed. C. F. Holmes and A. R. Landgrebe, Electrochemical Society, Pennington, NJ, 1997, pp. 109–115.
24 D. D. Wagman, W. H. Evans, V. B. Parker, I. Halow, S. M. Bailey and R. H. Schumm, *Natl. Bur. Stand. (U.S.)*, Tech. Note 270-4, 1969, p. 68.
25 A. Mabuchi, K. Tokumitsu, H. Fujimoto and T. Kasuh, *J. Electrochem. Soc.*, 1995, **142**, 3049.
26 T. Zheng, J. S. Xue and J. R. Dahn, *Chem. Mater.*, 1996, **8**, 389.
27 A. N. Dey, *Thin Solid Films*, 1977, **43**, 131.
28 D. Aurbach and Y. Ein-Eli, *J. Electrochem. Soc.*, 1995, **142**, 1746.
29 K. Kanamura, S. Shiraishi, H. Takezawa and Z. Takehara, *Chem. Mater.*, 1997, **9**, 1797.
30 R. Alcántara, F. J. Fernández Madrigal, P. Lavela, J. L. Tirado, J. M. Jiménez Mateos, R. Stoyanova and E. Zhecheva, *Chem. Mater.*, 1999, **11**, 52.
31 C. J. Pouchert, *The Aldrich Library of IR Spectra*, Aldrich Chemical Company, Milwaukee, WI, 1975, P5265-2 and E2625-8.
32 D. Aurbach, Y. Ein-Eli, O. Chusid, Y. Carmeli, M. Babai and H. Yamin, *J. Electrochem. Soc.*, 1994, **141**, 603.
33 I. A. Courtney, W. R. McKinnon and J. R. Dahn, *J. Electrochem. Soc.*, 1999, **146**, 59.

Paper 9/02060H